New Journal of Physics
The open–access journal for physics

From Maxwell demon to Brownian motor

C Van den Broeck[1], P Meurs[1] and R Kawai[2]

[1] Limburgs Universitair Centrum, B-3590, Diepenbeek, Belgium
[2] Department of Physics, University of Alabama at Birmingham, Birmingham, AL 35294, USA
E-mail: christian.vandenbroeck@luc.ac.be

New Journal of Physics **7** (2005) 10
Received 10 September 2004
Published 31 January 2005
Online at http://www.njp.org/
doi:10.1088/1367-2630/7/1/010

Abstract. Several versions of a hard disc microscopic ratchet are introduced and studied with molecular dynamics. While, at equilibrium, no rectification of the fluctuations takes place, a systematic motion appears when a temperature difference is applied to different units of the motor. In the limit of dilute gases, an exact analytic calculation of its properties is found to be in excellent agreement with molecular dynamics simulations.

Contents

PII: S1367-2630(05)86316-5

1. Introduction

Few stories in science have received so much ongoing attention from both the general public and the scientific community and have led to many, often confusing and sometimes acrimonious, debates as the second law of thermodynamics and its possible violation. While there exists a general consensus that the second law is obeyed in macroscopic systems, opinion is less clear cut when one deals with small-scale systems. In this respect, one usually refers to the problem of Maxwell demons, defined as non-macroscopic objects that violate the second law of thermodynamics [1]. In the original construction proposed by Maxwell [2], a demon-like device operates a door separating two compartments of a container, opening and closing it in such a way that only fast particles from one side and slow particles from the other side are allowed to pass, thereby 'spontaneously' generating a temperature gradient. Maxwell was apparently under the impression that such a construction might be possible, provided one were able to operate and manipulate at this small-scale level. However in the long debate that followed the introduction of the demon, several general arguments and subtle issues were pointed out by a series of other distinguished physicists. Smoluchowski [3] argued that the demon, being itself of small scale, could only function properly if it was not subject to thermal fluctuations, i.e., it had to be cooled at the expense of entropy production. Onsager [4] noted that microreversibility in Hamiltonian systems at equilibrium (canonical or micro-canonical ensemble) imply the property of detailed balance, meaning that any process and its time-reverse occur with the same probability, excluding any Maxwell-demon-like rectification. Szilard [5] and Brillouin [6] focused on the innocuous-looking assumption that one needs to know the speed of the particle and argued that the information process or measurement process would necessitate entropy production, off-setting any entropy decrease realized by the demon. This issue was settled by Landauer [7], who identified the erasure of information as the irreversible entropy-producing step. Feynman [8] proposed a detailed construction inspired by the discussion of Smoluchowski [3] (see figure 1), and performed an explicit calculation to show that the rectification can only take place if there is a temperature difference between the demon and the gas. His calculation indicates that work can indeed be extracted, reaching in fact Carnot efficiency, a result that was later refuted in [9, 10].

Today, the issue of Maxwell demons has become even more relevant than at the time of Maxwell. Firstly, with the recent breakthrough in the observation, manipulation and even the manufacture of small-scale physical, chemical and biological objects, the Maxwell construction is no longer a thought experiment but is now technologically feasible [11]. More generally, the physics, chemistry and biology of the nano and meso scale, a scale at which fluctuations cannot be ignored, will play a predominant role in the scientific and technological advances in the 21st century. Secondly, recent advances in statistical physics stress the relation between different levels of description, relating dynamical, probabilistic and thermodynamic concepts [12, 13]. Thirdly, the ever rapidly improving computer power allows extremely precise numerical experiments uncovering new aspects of the microscopic dynamics [14]. Finally, the issue of Maxwell demons is closely linked to the topic of Brownian motors, which has recently received considerable attention [15]. Brownian motors are small-scale asymmetric objects that are able to rectify thermal fluctuations because they operate under non-equilibrium constraints.

It is quite surprising to us that, despite the continuous quest for Maxwell demons, no exact microscopic analysis has ever been performed, apart from a few deserving attempts [16]–[21]. Our intention therefore is to construct such a model by a simplification of the Feynman model [22]. It should be amenable to extremely precise molecular dynamics simulations and even

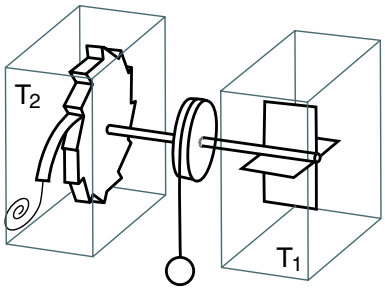

Figure 1. Schematic representation of the Feynman ratchet [8].

more importantly to an exact theoretical description. Discovery of such a model proceeded in various steps. The purpose of this paper is to record the history of this process. The new Brownian motor started its life under the form of a Maxwell demon, called Lucifera. Over several phases of evolution, involving Angelina, Motorina and Arrowina, it finally culminated in a set of Brownian motors, including Triangulita and Triangula, for which a full microscopic calculation and agreement with molecular dynamics simulations could be achieved.

2. Feynman ratchet

Let us first recall some details of the Feynman construction [8] (figure 1). He replaces the demon-like being selecting speeds from the original Maxwell proposal by a mechanical rectifier used in clockworks of all kinds, consisting of a ratchet with a pawl and a spring. The macroscopic mode of operation of such an object generates the impression that only clockwise rotations can take place since the pawl will block any counter-clockwise rotations. To drive the motion, Feynman rigidly links the ratchet to a set of blades that undergo collisions with the thermal particles. He shows that the rectification will only function for a transient time, after which the whole construction, and in particular the spring that retains the pawl, will eventually heat up to the same temperature as the particles. When the pawl lifts by thermal fluctuation, it will no longer prevent counter-clockwise fluctuations. To proceed, he generalizes the construction to a two-compartment system, with the possibility to keep the ratchet and blades at different temperatures. The subtlety of his quantitative analysis is revealed by the fact that one of his major conclusions, namely that this thermal motor can reach Carnot efficiency, turns out to be incorrect [9, 10].

An accurate microscopic study based on first principles, either analytical theory or computer simulation, is rather difficult for the original Feynman ratchet due to the presence of the spring and pawl. Almost all theoretical studies of this or related models are mesoscopic [16], with the prototype being a Brownian particle travelling in a one- or two-dimensional asymmetric potential. However, such stochastic models, usually based on Markovian Langevin dynamics, are mere toy images of the original model and bypass the fundamental issues involved in rectification. Our aim here is to provide an analysis, based on first principles, with a complementary analysis by microscopic theory and molecular dynamics simulations.

3. Lucifera

We first set out to construct a model whose microscopic dynamics can be simulated very accurately. In this respect, hard disc molecular dynamics simulation would clearly be an optimal

choice. Recent codes [14] are relatively fast while the only computational error is due to the round-off error of the computer. We will, without loss of generality, limit ourselves to a two-dimensional hard disc rather than a three-dimensional hard sphere system. With respect to the Feynman construction, however, we encounter another difficulty. Apart from the outright difficulty of modelling the construction with mechanical entities, hard disc simulations cannot be combined efficiently with potential interactions. On second thoughts, the pawl with spring is not essential in the construction, even though it has a visual and intuitive appeal, especially to the layperson. But any device that breaks spatial symmetry is a candidate rectifier. Proceeding with further simplification of the Feynman model, it will be convenient to replace the rotational degree of freedom with a translational one, with periodic boundary conditions. When we attempt to propose an asymmetric ratchet-like mechanical object, we again encounter a technical difficulty. A ratchet has sharp corners, rendering simulations with hard disc dynamics extremely difficult. In fact, the only collisions that can be treated easily are discs with discs or discs with a flat object, but a collision rule between a disc and a sharp corner is not obvious. It must be defined such that no basic law of physics is violated [17]. To avoid corners, we can imagine a flat sheet that covers the entire width of the system, reminiscent of the adiabatic piston [19, 20].

However, for rectification to take place, two other ingredients need to be provided: the sheet should allow the passage of particles if it is not to hamper its own motion. Conservation of total momentum implies that the system when initially at rest (total momentum zero) will remain so for all times. If the sheet cannot be crossed by particles, then a sustained motion will be impossible. The second ingredient is that the object needs to be asymmetric. The first requirement can be met by assuming that the sheet has a potential of interaction, that is infinitely sharp leading to an instantaneous collision, as is usual with hard core interactions, but does not have an infinite height. More precisely, when the relative kinetic energy of the motion of a particle versus the sheet exceeds a threshold U, the particle and sheet surmount the barrier and instantaneously pass unhampered (with unchanged velocities) through each other. Otherwise a perfectly reflecting collision (with rules dictated by conservation of energy and momentum) takes place. This semi-transmissive sheet also suggests an easy procedure to generate an asymmetry: consider a second sheet at a rigidly fixed distance from the first one, but characterized by a different threshold potential.

We thus finally arrive at Lucifera illustrated in figure 2(a), whose construction we now review. She consists of two parallel semi-transmissive sheets (total mass M) at a fixed distance d from each other, which can freely move with a speed V along the horizontal x-axis. Their joint motion is induced by collisions with a gas of hard discs (diameter $\sigma = 1$, mass $m = 1$, speed $\vec{v} = (v_x, v_y)$, number of particles = N), which is enclosed in the same cylinder at equilibrium at temperature $T = 1$ (the Boltzmann constant is $k_B = 1$ by an appropriate choice of the energy unit). Boundary conditions are periodic at left and right and periodic or perfectly reflecting on top and bottom. Note that the system in its totality is isolated so that it would be more correct to refer to a microcanonical ensemble with a given total energy. However, in view of the large number of particles used in the simulations, the velocity $\vec{v}$ of each particle is in good approximation Maxwellian and the second moment can be used to identify a temperature $mv^2/2 = k_B T$. The sheets of Lucifera undergo perfectly reflecting collisions with the hard disc when the relative velocity of sheet and particle upon touching each other is below a specific threshold, while the particles move unhampered through the sheets when the relative velocity is higher than this threshold. More precisely, the post-collisional velocities (indicated with primes) are obtained in terms of the pre-collisional velocities on the basis of conservation of energy and

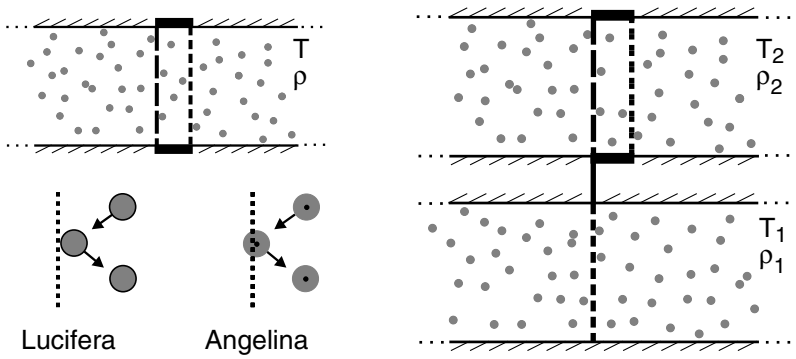

Figure 2. Left, schematic representation of Lucifera and Angelina. They both have the same geometric structure, consisting of two semi-transparent sheets at a fixed distance from each other, both of which are free to move without friction along the axis of the cylinder. They differ in the collision rule with the disc: see insets. Right, Motorina, corresponding to Angelina receiving a third semi-transparent sheet connected rigidly to the previous two sheets and located in a second cylinder at a different temperature.

momentum:

$$\tfrac{1}{2}MV^2 + \tfrac{1}{2}mv^2 = \tfrac{1}{2}MV'^2 + \tfrac{1}{2}mv'^2, \qquad MV + mv_x = MV' + mv'_x, \qquad v_y = v'_y. \tag{1}$$

This set of equations has two solutions. The 'trivial' one

$$V' = V, \qquad \vec{v}' = \vec{v}, \tag{2}$$

which is chosen when the relative speed $|V - v_x|$ of particle and sheet moving towards each other, exceeds the threshold of the sheet. The other solution:

$$v'_x = \frac{m-M}{M+m}v_x + \frac{2M}{M+m}V_x, \qquad v'_y = v_y, \qquad V' = \frac{M-m}{M+m}V + \frac{2m}{M+m}v_x, \tag{3}$$

corresponds to a perfect elastic collision and is selected when the relative speed is below the threshold.

We turn now to the result of the simulations. In figure 3(a), we show the average over 5000 trajectories of Lucifera's motion. One clearly notices a systematic net displacement of Lucifera to the left. So Lucifera is a genuine Maxwell demon: her motion is in violation of the second law! Indeed the system considered here is an isolated equilibrium system and rectification of thermal fluctuations is impossible. If one were to attach a small load to Lucifera, she would be able to pull it up while cooling down the Enskog gas in which she lives. Another more appropriate way to state the inconsistency here is that Lucifera is violating detailed balance. When the latter condition is satisfied, any transition between two states is equally likely to occur in both directions, excluding the possibility of systematic biased motion. As expected, violation of the second law is flawed and related to a subtle mistake in the implementation of the collision rule, which is discussed in the next section. Fortunately, this very same mistake suggests a correction that will allow us to move beyond the limitations of Lucifera.

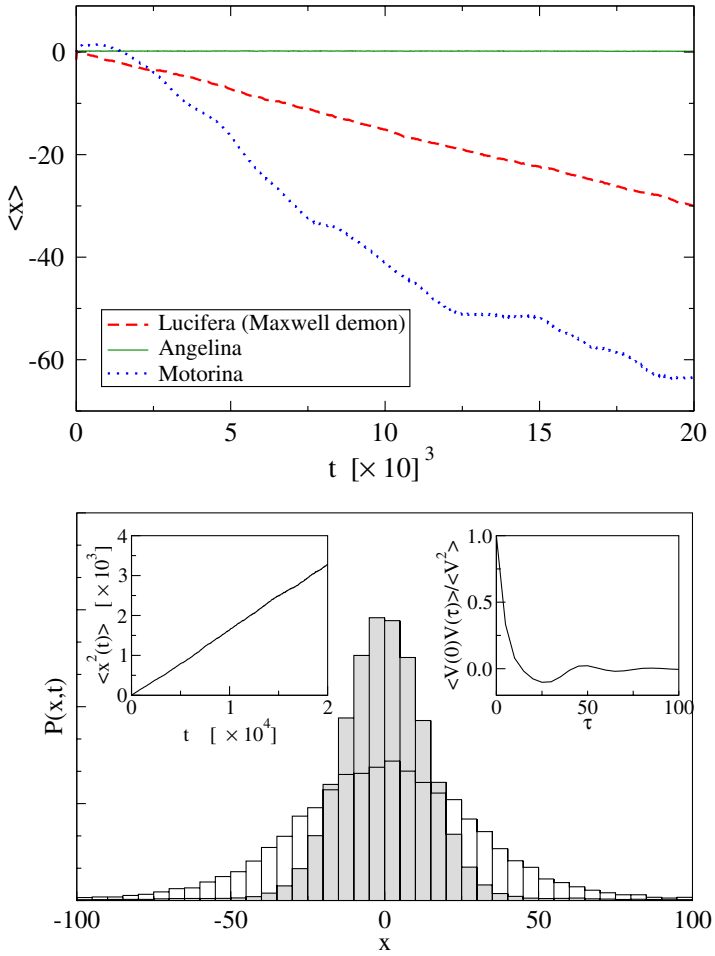

Figure 3. Top, the dashed line corresponds to the Maxwell demon (Lucifera, figure 2(a)) discussed in the main text. The parameter values are $M/m = 25$, $T = 1$, $N = 250$ and energy thresholds $U = 1.0$ and 0.5 for the left and right sheets, respectively. All results are averages of 5000 runs in a system of size 68×20. The full line is the (unbiased) motion that appears when the collision rule between discs and sheets are corrected (Angelina). The lower curve corresponds to Motorina (figure 2(b)). The parameter values of the lower curve are $N_1 = N_2 = 250$, $M/m = 5$, $T_1 = 1.9$, $T_2 = 0.1$ and thresholds $U = 10.0$, 0.1 in the upper cylinder and $U = 0.1$ in the lower cylinder. In all simulations, a distance $d = 2$ between the sheets is used. Bottom, probability density $P(x, t)$ for the position x of Angelina at time $t = 1000$ (shaded) and 4000 (open). Inset left, mean square displacement versus time. Inset right, velocity correlation function. The thresholds are $U = 1.0$ and 0.5, the number of particles is $N = 250$, and the mass ratio is $M/m = 25$. Averages of 1000 runs are taken.

4. Angelina

Lucifera's motion originates from an erroneous prescription of the collision process when the relative speed of the disc with respect to the sheet exceeds the corresponding threshold. The

potential of interaction between disc and sheet operates when they touch each other. But this cannot be reconciled with the fact that the hard discs have a finite radius, hence they do not cross the sheet instantaneously, even when the sheets are infinitesimally thin. In fact, if the interaction potential is activated when the hard disc crosses the sheet, both the sheet and disc would have to slow down during this crossing since part of their kinetic energy is transformed into potential energy. This looks like a disaster from the point of view of the simulations since taking into account finite potential energy more or less kills the efficiency of the code. There is however a simple trick to circumvent the problem that will furthermore pave the way for the other models. We can assume that the interaction of the sheet is only with the centre of the hard disc (see figure 2(a)). Hence the centre of the particles either bounces back in a perfectly elastic instantaneous collision from the sheet below threshold, or they cross the sheet, which is now also an instantaneous event, when the relative speed exceeds the threshold. Hence everything is again reduced to hard core collisions. The previously mentioned collision laws, equations (2) and (3), remain valid, but they are applied when the centre of the disc hits the sheet. To stress the distinction from the previous erroneous prescription of the collisions, the corrected form of Lucifera will be called Angelina, see figure 2(a).

Turning to the simulations, we find that Angelina, even though she has a left–right asymmetry, performs an unbiased motion in agreement with the property of detailed balance as shown in figure 3(a). For large enough times, the motion converges to plain Brownian motion. Figure 3(b) shows that the probability density for the displacement of Angelina after a long time interval (1000 and 4000 time steps) is clearly Gaussian within the numerical accuracy. The Gaussian spreads out further as time goes on. We plot the mean-square displacement as a function of time in the left inset to figure 3(b). One clearly identifies a linear law $\langle x^2(t)\rangle = 2Dt$ with D the diffusion coefficient. We have also included in figure 3(b) the velocity autocorrelation function (right inset), whose decay is not exponential, with an oscillatory long time tail probably induced by complicated hydrodynamic effects [23].

5. Motorina

Angelina is clearly an asymmetric object when her two thresholds are not equal. Nevertheless, she is, as we illustrated in the previous section, a 'boring' Brownian object when sitting in a system at equilibrium. No energy can be extracted from her. This is to be contrasted with the so-called Brownian motors, where rectification is possible because they operate under a non-equilibrium constraint. To put Angelina in this new context, we note that she could perform the role of the ratchet in the Feynman construction. In order to include a non-equilibrium component, we follow Feynman's idea and introduce a second reservoir at a different temperature. We attach to Angelina another semi-transparent sheet, rigidly linked to the previous body, but sitting in this second reservoir, see figure 2(b). To make the distinction with Angelina, we will refer to this new Brownian motor construction as Motorina. In contrast to Angelina, we expect Motorina to be 'alive'. She breaks, by construction, spatial left–right symmetry, while simultaneous contact with two reservoirs at different temperatures implies that the more stringent symmetry of detailed balance, characteristic for an equilibrium system, is also broken. This is precisely what is observed, as shown in figure 3(a). The resulting systematic speeds are unfortunately rather small, so we have focused on a choice of thresholds that more or less optimizes the average speed. Apart from the important simplifications with respect to the Feynman construction, we

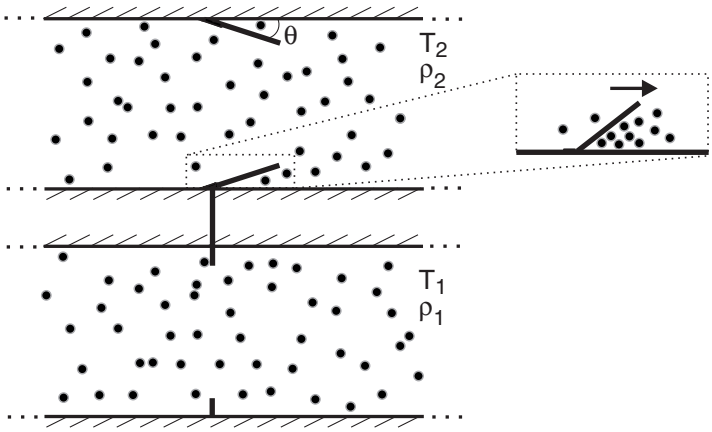

Figure 4. Schematic representation of Arrowina. Inset, at high densities, particles tend to accumulate underneath the inclined sheet when it moves to the right, thereby hampering its motion.

note another essential difference. The momentum of the Feynman ratchet is not conserved along its rotational direction of motion, because the wall on which the spring is attached exchanges momentum with the motor. Note that this is also the case in the standard models of Brownian motors, in particular the flashing or rocking ratchet, in which a background potential is available, with which momentum can be exchanged. In Motorina, we have neither background potential nor wall. Hence momentum along the horizontal x-axis is conserved, a feature which has a profound theoretical implication as we will discuss in more detail later. At this point, we mention another consequence of this feature, namely that the observed systematic motion of Motorina must be compensated by a counter-motion of the gas in which she is embedded. In other words, the motor also operates as a pump.

6. Arrowina

Motorina is essentially a one-dimensional construction that is able to rectify thermal fluctuations. There are however two reasons why the model is not entirely satisfactory. Firstly, the observed systematic motion is not easy to detect. Even after optimization of the threshold values, one has to make an average over a large number of runs to filter out the strong underlying Brownian motion. Running for much longer times, instead of averaging, is not an alternative for another reason, an issue to which we will also return in much more detail later on. The single degree of freedom of Motorina established a thermal contact between the two reservoirs, so that, in the course of time, the temperatures in both reservoirs will eventually equalize, and the systematic motion will eventually disappear. This could be avoided by working with large reservoirs, an option which is however computationally very expensive. To summarize, the first main criticism of Motorina is that her systematic speed is too slow, in comparison to her thermal agitation. The second problem is more poignant: we are not able to explain, even on an intuitive basis, the mechanism behind her systematic motion.

We hence turn to another construction called Arrowina, which is now rendered possible by the new prescription of collisions between sheets and discs. Corners need no longer to be avoided. As represented in figure 4, Arrowina consists of two rigidly linked small sheets, not

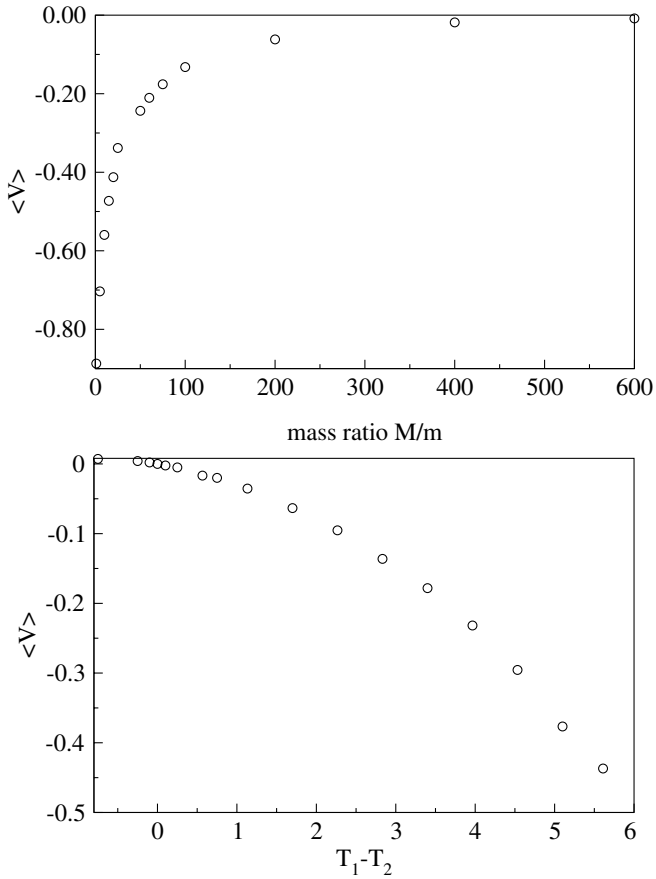

Figure 5. Top, average velocity of Arrowina as a function of its mass ratio M/m. The temperatures of the lower and upper reservoirs are $T_1 = 5.2$ and $T_2 = 0.1$, respectively. Bottom, average velocity of Arrowina as a function of the initial temperature difference. The mass ratio is $M/m = 25$ and $T_1 + T_2 = 2$. The other common parameter values are the system size 68×20, the number of particles $N_1 = 150$, $N_2 = 700$ and angle $\theta = 0.05^\circ$. All data points are averages of 2000 runs.

covering the entire width of the system and no longer semi-transparent for the discs. They move together as a single entity with a single degree of freedom corresponding to a motion along the x-axis. One sheet, which we will call the paddle, is perpendicular to the x-direction, while the other one, which we will call the ratchet, makes an angle θ with the horizontal. The sheets sit in two different reservoirs, and collide with the centre of hard discs, which are prepared in each reservoir in an equilibrium state, but possibly at a different temperature. The boundary conditions are periodic left and right, but, and this is essential, perfectly reflecting up and down. The ratchet sheet glides along the sidewalls. The idea is that, when $\theta \neq \pi/2$, it acts as a ratchet hampering her own motion by trapping particles, see inset to figure 4. Its asymmetry combined with a temperature difference is expected to generate motion. Since the asymmetry can now be tuned, we expect higher systematic speeds. This expectation is borne out by the numerical experiments, see figure 5. Note in particular that high speeds require a very strong asymmetry with θ close to 0° and at the same time rather high densities of the gas.

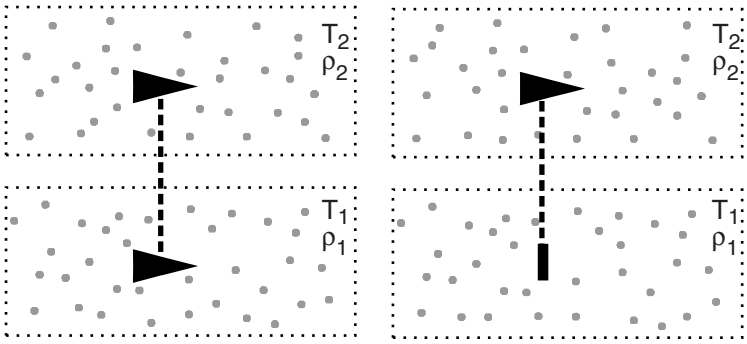

Figure 6. Left, schematic representation of Triangula. The motor is constrained to move along the horizontal x-direction without rotation or vertical displacement. The host gas consists of hard discs whose centres collide elastically with the engine parts. The shape of the triangle is determined by the apex angle $2\theta_0$ and the vertical cross-section L. Periodic boundary conditions are used in the computer simulations. Right, an analogous construction, referred to as Triangulita, in which the symmetry between the reservoirs is broken.

While the systematic motion of Arrowina is very pronounced for certain values of the parameters, she still suffers from the same predicament as Motorina: we do not have a clear understanding of the rectification mechanism. It is true that the motion of Arrowina in a gas at high density is in agreement with our macroscopic intuition, see inset to figure 4. When the temperature is high in the paddle reservoir, she moves in the direction of 'least friction', namely the one in which the ratchet-sheet does not trap particles. Unfortunately, this argument is misleading and unreliable. As we will show next, the models that are discussed here lie outside the realm of linear irreversible thermodynamics and macroscopic intuition cannot be relied on. In the case of Arrowina and Motorina, the explanation is furthermore complicated by the fact that correlations involving recollisions, in particular those of the gas particles trapped between the ratchet and the boundary, presumably play a dominant role. Avoiding the effect of recollisions is clearly an important requirement if one is to hope for an exact theoretical analysis.

7. Triangula and Triangulita

In our search for a model that can be solved analytically, we note that many of the exactly solvable models in statistical mechanics involve dilute ideal gases. In the context of our present discussion, the appropriate limit would be to consider the case in which the density of the hard disc gases becomes very low and the reservoirs very large so that one effectively reaches the limit of an ideal gas. But if we want to invoke the simplicity of the molecular chaos hypothesis, we also need to avoid recollisions of gas particles with the motor units. This can only be guaranteed when units are convex. This implies that our units cannot be flat, but need to have an inner core surrounded by a closed convex shell. One of the simplest asymmetric convex objects is a triangle. Hence we are led to the construction schematically represented in figure 6(a). We will call this motor Triangula. It consists of two rigidly linked triangular units moving as a whole along the horizontal x-axis. Each unit sits in a separate infinitely large reservoir containing an

ideal gas. When the temperatures in the two reservoirs are different, we have the ingredients of a Brownian motor and we expect the appearance of a systematic motion. Because Triangula has the additional symmetry that the units have the same shape in both reservoirs, we will also study the motor consisting of a triangular unit in one reservoir and a flat sheet in the other as depicted in figure 6(b), referred to as Triangulita.

As far as the molecular dynamics simulation is concerned, we obviously work with reservoirs that are relatively large but of finite size. For comparison with the theory given below, we will focus on the low-density case, but we will, for reasons of obvious interest, also explore the behaviour at higher density. Before doing so, we turn to one of the major achievements, namely the presentation of a microscopically exact analysis of Triangula and Triangulita.

8. Expansion of the Boltzmann equation

Let us first repeat the basic idea. The motor consists of two or more units that move as a rigidly linked whole along a specified direction x with speed V. The units are all convex and reside in different infinitely large compartments i, filled with ideal gases at equilibrium within each compartment, with particle mass m, density ρ_i and Maxwellian velocity distribution ϕ_i at temperature T_i:

$$\phi_i(v_x, v_y) = \frac{m}{2\pi k_B T_i} \exp\left(\frac{-m(v_x^2 + v_y^2)}{2k_B T_i}\right). \tag{4}$$

Due to the absence of any pre-collisional correlations between the speed V of the motor and that of the impinging particles, the probability density $P(V, t)$ for the speed $\vec{V} = (V, 0)$ obeys a Boltzmann–Master equation [24]:

$$\frac{\partial P(V,t)}{\partial t} = \int \mathrm{d}V' \left[W(V|V')P(V',t) - W(V'|V)P(V,t)\right]. \tag{5}$$

$W(V|V')$ is the transition probability per unit time for the motor to change speed from V' to V due to the collisions with gas particles in the compartments. To proceed, the explicit expression of the transition probabilities needs to be specified. This will require a few steps of preparation.

Firstly, the shape of the closed convex motor unit in reservoir i can be defined by the normalized probability density $F_i(\theta)$ such that $F_i(\theta)\,\mathrm{d}\theta$ is the fraction of its outer surface that has a tangent between θ and $\theta + \mathrm{d}\theta$ as presented in figure 7. The angle θ is measured counter-clockwise from the horizontal x-direction. The perimeter will be denoted by S_i. Note that $\langle \sin\theta \rangle = \langle \cos\theta \rangle = 0$, where the average is with respect to $F_i(\theta)$, a property resulting from the requirement that the object is closed. In the case of Triangula, the shape functions F_1 and F_2 are the same in both compartments. Furthermore, θ can only take three values, corresponding to the angles formed by the three sides of the triangle, namely θ_0, $\pi - \theta_0$ and $3\pi/2$. Taking into account the relative length of each of the sides versus the perimeter, one finds:

$$F_1(\theta) = F_2(\theta) = \frac{2\delta\left[\theta - (3\pi/2)\right]\sin\theta_0 + \delta\left[\theta - \theta_0\right] + \delta\left[\theta - (\pi - \theta_0)\right]}{2(1 + \sin\theta_0)}. \tag{6}$$

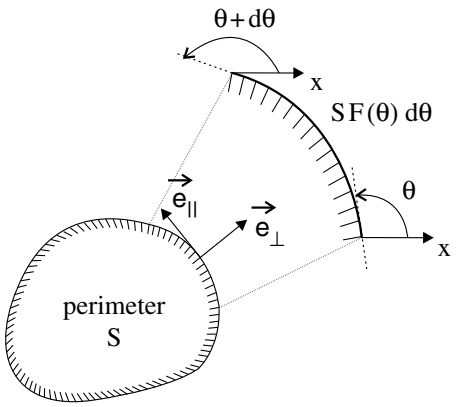

Figure 7. A closed and convex object with perimeter S. The length of the surface with an orientation between θ and $\theta + \mathrm{d}\theta$ is $SF(\theta)\,\mathrm{d}\theta$, defining the form factor $F(\theta)$.

Consider now the collision between a gas particle (pre-collisional velocity $\vec{v}' = (v'_x, v'_y)$) and the motor, with pre-collisional velocity $\vec{V}' = (V', 0)$, at a location of the surface of one of the units with orientation θ. The normal and tangential vector to this section are $\vec{e}_\perp = (\sin\theta, -\cos\theta)$ and $\vec{e}_\parallel = (\cos\theta, \sin\theta)$ respectively, see figure 7. To find the post-collisional velocities, we note that the total energy and momentum in the x-direction are conserved (the binding force that keeps the motor on its track parallel to the x-direction is orthogonal to this direction, hence it performs no work and it does not affect the momentum in the x-direction):

$$\tfrac{1}{2}MV^2 + \tfrac{1}{2}mv^2 = \tfrac{1}{2}MV'^2 + \tfrac{1}{2}mv'^2, \qquad MV + mv_x = MV' + mv'_x. \tag{7}$$

Furthermore, we assume that the interaction is due to a (short-range) central force, implying that the motor exerts no force on the impinging particle in the direction parallel to its surface. Hence the component of the momentum of the gas particle along the contact surface of the object is also conserved:

$$\vec{v}' \cdot \vec{e}_\parallel = \vec{v} \cdot \vec{e}_\parallel. \tag{8}$$

This yields for the post-collisional velocities:

$$\begin{aligned} V &= V' + \frac{2(m/M)\sin^2\theta}{1 + (m/M)\sin^2\theta}\left(v'_x - V' - v'_y\cot\theta\right), \\ v_x &= v'_x + \frac{2\sin^2\theta}{1 + (m/M)\sin^2\theta}\left(V' - v'_x + v'_y\cot\theta\right), \\ v_y &= v'_y + \frac{2\sin\theta\cos\theta}{1 + (m/M)\sin^2\theta}\left(V' - v'_x + v'_y\cot\theta\right). \end{aligned} \tag{9}$$

The final step consists in estimating the frequency for all possible types of collisions. This can be done following the usual procedure familiar from kinetic theory. We consider one specific

type of event, namely collisions with initial speeds in a volume $\mathrm{d}\vec{v}'$ centred on $\vec{v}'$, hitting the motor with pre-collisional speed $\vec{V}'$ on a section of length $\mathrm{d}l$ with orientation θ during a short time interval $\mathrm{d}t$. The average number of such collisions is equal to the average number of particles within the specified speed range in a rectangle with basis $\mathrm{d}l$ and height $(\vec{V}' - \vec{v}') \cdot \hat{e}_\perp \, \mathrm{d}t$, namely $\rho_i \phi_i(v'_x, v'_y)(\vec{V}' - \vec{v}') \cdot \hat{e}_\perp \, \mathrm{d}\vec{v}' \, \mathrm{d}l \, \mathrm{d}t$. Furthermore, since the pre-collisional relative speed must be positive, we have the additional condition $(\vec{V}' - \vec{v}') \cdot \hat{e}_\perp > 0$. By integrating over all velocity components, perimeter, compartments and switching to the angular variable by $\mathrm{d}l = S_i F_i(\theta) \, \mathrm{d}\theta$, one obtains the total transition probability per unit time:

$$W(V|V') = \sum_i \int_0^{2\pi} \mathrm{d}\theta \, S_i F_i(\theta) \int_{-\infty}^{+\infty} \mathrm{d}v'_x \int_{-\infty}^{+\infty} \mathrm{d}v'_y \rho_i \phi_i(v'_x, v'_y) \times (\vec{V}' - \vec{v}') \cdot \hat{e}_\perp \Theta[(\vec{V}' - \vec{v}') \cdot \hat{e}_\perp] \times \delta \left[V - V' - \frac{2(m/M) \sin^2 \theta}{1 + (m/M) \sin^2 \theta} (v'_x - v'_y \cot \theta - V') \right], \tag{10}$$

where Θ is the Heaviside step function. The δ function in equation (10) selects appropriate particle velocities yielding, according to equation (9), the post-collisional speed V for the motor.

For the ensuing calculation, it is advantageous to introduce the transition probability $W(V'; r) = W(V|V')$, defined in terms of the jump amplitude $r = V - V'$. One can then rewrite the Boltzmann equation as follows:

$$\frac{\partial P(V, t)}{\partial t} = \int W(V - r; r) P(V - r, t) \, \mathrm{d}r - P(V, t) \int W(V; -r) \, \mathrm{d}r. \tag{11}$$

An exact solution of the Boltzmann–Master equation is out of the question, even at the steady state. To make progress, a perturbative solution is necessary. Since we expect that the rectification disappears in the limit of a macroscopic motor, a natural expansion parameter is the ratio of the mass m of the gas particle over the mass M of the object. More precisely, we will use $\varepsilon = \sqrt{m/M}$ as the expansion parameter. Note however that the parameter M will also appear implicitly in the speed V. Indeed, we expect that the object will, in the stationary regime, exhibit thermal fluctuations at an effective temperature T_{eff}, i.e., $\frac{1}{2} M \langle V^2 \rangle = \frac{1}{2} k_B T_{\mathrm{eff}}$. To take this into account, we switch to a dimensionless variable x of order 1:

$$x = \sqrt{\frac{M}{k_B T_{\mathrm{eff}}}} V. \tag{12}$$

The effective temperature will be determined by the self-consistent condition $\langle x^2 \rangle = 1$. The Taylor expansion of the r.h.s. of the Boltzmann equation (11) with respect to the jump amplitude leads to an equivalent expression under the form of the Kramers–Moyal expansion:

$$\frac{\partial P(x, t)}{\partial t} = \sum_{n=1}^{\infty} \frac{(-1)^n}{n!} \left(\frac{\mathrm{d}}{\mathrm{d}x} \right)^n \{ A_n(x) P(x, t) \}, \tag{13}$$

with rescaled jump moments, $A_n(x)$, defined as

$$A_n(x) = \left(\sqrt{\frac{M}{k_B T_{\mathrm{eff}}}} \right)^n \int r^n W(V; r) \, \mathrm{d}r. \tag{14}$$

Equivalently, and of more interest to us, the following set of coupled equations determine the moments $\langle x^n \rangle = \int x^n P(x,t)\,\mathrm{d}x$:

$$\partial_t \langle x \rangle = \langle A_1(x) \rangle, \tag{15}$$

$$\partial_t \langle x^2 \rangle = 2\langle x A_1(x) \rangle + \langle A_2(x) \rangle, \tag{16}$$

$$\cdots$$

The exact solution of this coupled set of equations is as hopeless and equally difficult as the full Boltzmann–Master equation. However, a Taylor expansion in ε shows that the equations are no longer fully coupled and the calculation of a moment up to a finite order in the stationary regime reduces, in principle, to a simple (but in practice tedious) algebraic problem.

Turning to the specific case of Triangula, we first note that the integrals over the angle and speed in the transition probability can be easily performed explicitly, with the result:

$$W(V;r) = L \sum_i \rho_i \sqrt{\frac{m}{2\pi k_B T_i}} \times \begin{cases} r \sin\theta_0 \left(\dfrac{1+\epsilon^2 \sin^2\theta_0}{2\epsilon^2 \sin^2\theta_0} \right)^2 \exp\left[-\dfrac{m \sin^2\theta_0}{2k_B T_i} \left(V - \dfrac{1+\epsilon^2 \sin^2\theta_0}{2\epsilon^2 \sin^2\theta_0} r \right) \right] & \text{if } r > 0, \\ -r \left(\dfrac{1+\epsilon^2}{2\epsilon^2} \right)^2 \exp\left[-\dfrac{m}{2k_B T_i} \left(V - \dfrac{1+\epsilon^2}{2\epsilon^2} r \right) \right] & \text{if } r < 0. \end{cases} \tag{17}$$

Hence, the following series expansion in ε is obtained for the two lowest jump moments:

$$A_1(x) = -\sum_{i=1,2} 4L \sqrt{\frac{k_B}{2\pi m}} \rho_i \sqrt{T_i} (1+\sin\theta_0) x \varepsilon^2 + \sum_{i=1,2} L \sqrt{\frac{k_B}{m}} \frac{\rho_i T_i}{\sqrt{T_{\mathrm{eff}}}} (1-\sin^2\theta_0) \left(\frac{T_{\mathrm{eff}}}{T_i} x^2 - 1 \right) \varepsilon^3 + O(\varepsilon^4), \tag{18}$$

$$A_2(x) = \sum_{i=1,2} 8L \sqrt{\frac{k_B}{2\pi m}} \frac{\rho_i T_i^{3/2}}{T_{\mathrm{eff}}} (1+\sin\theta_0) \varepsilon^2 + O(\varepsilon^3). \tag{19}$$

From equation (18), together with equation (15), we immediately recognize that, to lowest order in ε, the first and second moment are decoupled. Furthermore, the first moment equation reduces to a linear relaxation law, which, written in the original variable, reads $M \partial_t \langle V \rangle = -\gamma \langle V \rangle$, with

$$\gamma = 4L \sqrt{\frac{k_B m}{2\pi}} (1+\sin\theta_0)(\rho_1 \sqrt{T_1} + \rho_2 \sqrt{T_2}). \tag{20}$$

At this level of the perturbation, the steady-state speed of the object is obviously zero. We conclude that no rectification takes place in the regime of linear response. Turning to the second moment, we note that the effective temperature T_{eff} follows from the self-consistent steady-state

condition $\langle x^2 \rangle = 1$. This implies, at this lowest order in ε, see equations (17) and (19), that

$$T_{\text{eff}} = \frac{\rho_1 T_1^{3/2} + \rho_2 T_2^{3/2}}{\rho_1 \sqrt{T_1} + \rho_2 \sqrt{T_2}}. \tag{21}$$

At the next order of perturbation in $\sqrt{m/M}$, noise and non-linearity become intertwined, while at the same time the Gaussian nature of the white noise is lost, a feature well known from the Van Kampen $1/\Omega$ expansion [25]. At this order, the equation for the average velocity is coupled to the second moment. Inserting $\langle x^2 \rangle = 1$ into equations (15) and (18) and returning to the original variable V, one readily finds at the steady state:

$$\langle V \rangle_{\text{Triangula}} = \rho_1 \rho_2 (1 - \sin\theta_0) \frac{\sqrt{2\pi k_B m}}{4M} \frac{(T_1 - T_2)(\sqrt{T_1} - \sqrt{T_2})}{\left[\rho_1 \sqrt{T_1} + \rho_2 \sqrt{T_2}\right]^2}. \tag{22}$$

This speed vanishes in the 'macroscopic' limit $M \to \infty$ as $\langle V \rangle \sim 1/M$. The fact that the combination of both asymmetry and temperature gradient is required to generate systematic motion is also contained in equation (22). If either $T_1 = T_2$ or $\theta_0 = \pi/2$ (the triangle becomes a bar and thus the asymmetry disappears), the average velocity vanishes. We furthermore observe from equation (22) that the speed of Triangula depends on the densities by their ratio ρ_1/ρ_2, with a maximum at $\rho_1/\rho_2 = \sqrt{T_2/T_1}$.

We turn now to our other model called Triangulita, see figure 6(b). The vertical bar in one reservoir mimics the blades in the original Feynman construction, while the triangle in the other reservoir is the asymmetric object replacing the needlessly complicated construction of the ratchet with pawl. Following a similar calculation, the drift speed of Triangulita to lowest order in ε is found to be

$$\langle V \rangle_{\text{Triangulita}} = \rho_1 \rho_2 (1 - \sin^2\theta_0) \frac{\sqrt{2\pi k_B m}}{2M} \frac{(T_1 - T_2)\sqrt{T_1}}{[2\rho_1 \sqrt{T_1} + \rho_2 \sqrt{T_2}(1 + \sin\theta_0)]^2}. \tag{23}$$

At first, this result appears to be similar to the one for Triangula. But the behaviour is very distinct with respect to the applied temperature difference. In fact, Triangulita has the more familiar behaviour: the direction of the net motion reverses when the temperature difference changes sign. In other words, equilibrium (the state with equal temperatures) is a point of flux reversal. Triangula behaves in a different way: its speed exhibits a parabolic minimum as a function of the temperature, with zero speed at equilibrium. This peculiar behaviour originates from the permutational symmetry of the identical motor units, implying that the speed must be invariant under the interchange of T_1, ρ_1 with T_2, ρ_2.

We finally note that one can, in both models, increase the asymmetry of the triangular unit(s) to generate a maximum drift speed. This maximum is reached in the limit $\theta_0 \to 0$ of (an) infinitely elongated and sharp triangle(s).

9. Molecular dynamics versus theory

We are now ready for the crucial test, namely a direct confrontation between theory and molecular dynamics for Triangula and Triangulita. To do so, we consider low densities, $\rho \approx 0.0022$, such that the Enskog gases have in good approximation the properties of dilute gases [26]. We start by

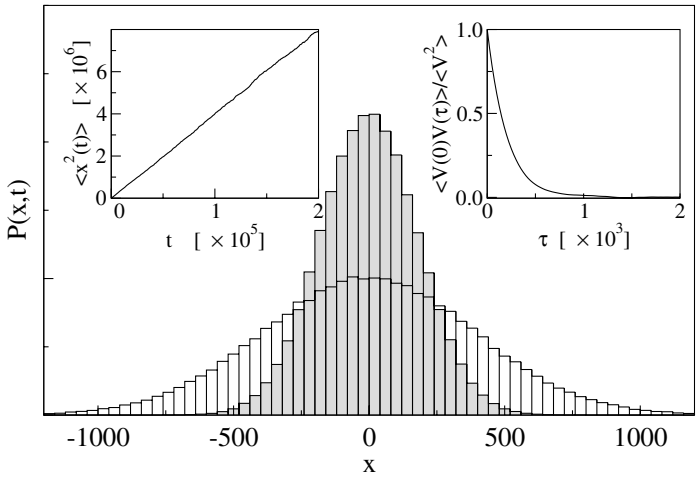

Figure 8. Probability density $P(x, t)$ for the position x of Triangula at times $t = 1000$ (shaded) and 4000 (open). Inset left: mean square displacement versus time. Inset right: velocity correlation function. Parameter values: system size 1800×450, temperatures $T_1 = T_2 = 1$, number of particles $N_1 = N_2 = 1800$, mass ratio $M/m = 10$, apex angle $2\theta_0 = \pi/18$ and vertical cross-section $L = 6.6$.

checking the properties of Triangula at equilibrium, $T_1 = T_2$. In agreement with the theory and the general principles of statistical mechanics and thermodynamics, Triangula does not develop any systematic speed. On a not too short time scale, her motion converges to plain Brownian motion. As shown in figure 8, the probability density for her displacement after a sufficiently long time interval (1000 and 4000 time steps) is clearly Gaussian within the numerical accuracy. The Gaussian spreads out further as time goes on. We plot the mean square displacement as a function of time in the left inset to figure 8. One clearly identifies a linear law $\langle x^2(t)\rangle = 2Dt$ with $D = 19.81$ the diffusion coefficient. We have also included in figure 8 the velocity autocorrelation function (right inset), whose decay is almost perfectly exponential, with time constant $(\gamma/M)^{-1} = 200.80$, hence ($M = 10$) the linear friction coefficient is $\gamma = 4.98 \times 10^{-2}$, in good agreement with the theoretical prediction, see equation (20): $\gamma = 5.04 \times 10^{-2}$. Note that the observed values of γ and D are consistent with the Einstein relation:

$$D = \frac{k_B T}{\gamma} = 20.08. \tag{24}$$

Turning to the non-equilibrium situation, a collection of results, including the theoretical predictions of (22) and (23), and results from molecular dynamics simulations are summarized in figure 9. The agreement is quite spectacular, especially taking into account that (a) there are no free adjustable parameters, (b) the theoretical result is the first term in a perturbation expansion in $\sqrt{m/M}$, (c) for the system size that is used, we expect significant finite-size effects (particles and in particular sound waves can easily travel around the system and reimpact on the motor). A similar agreement is found for the other model Triangulita. We have thus attained our primary goal, namely the introduction of a microscopic model for a Brownian motor that can be analysed in full analytic detail with results in agreement with a very precise molecular dynamics simulation. It vindicates the absence of rectification in equilibrium and gives a detailed

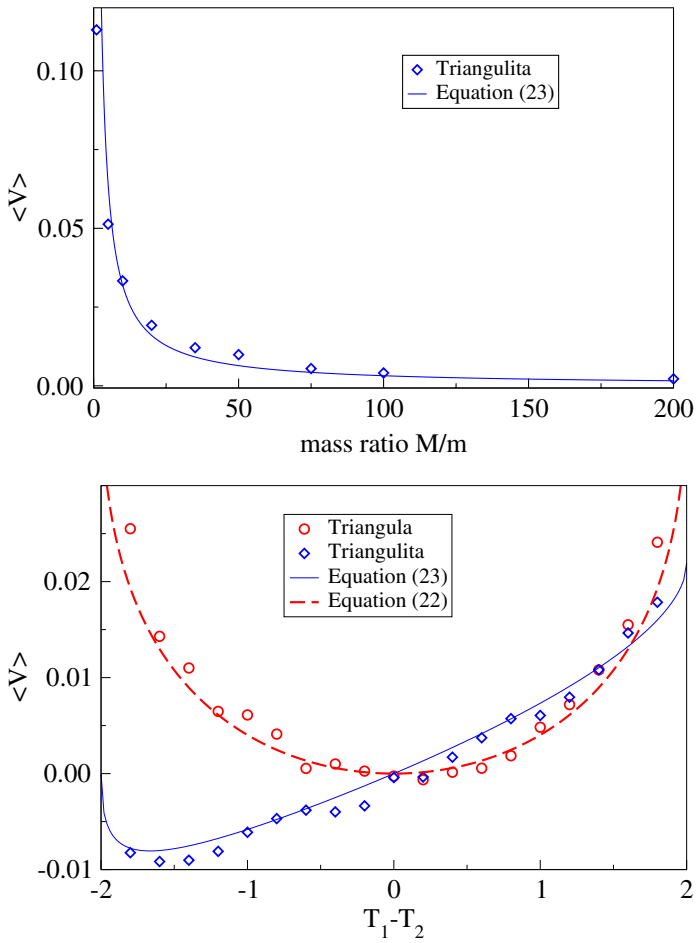

Figure 9. Top, average velocity of Triangulita as a function of its mass M. The following parameter values are used: system size 1200×300, particle numbers $N_1 = N_2 = 800$ ($\rho_1 = \rho_2 = 0.0022$), temperatures $T_1 = 1.9$ and $T_2 = 0.1$, apex angle $\theta_0 = \pi/18$ and vertical cross-section $L = 1$. All data points are averages over 2000 runs. The line corresponds to the theoretical prediction based on the perturbative solution of the Boltzmann equation, cf formula (23). Bottom, average speed of motors Triangula and Triangulita as a function of the initial temperature difference $T_1 - T_2$ ($T_1 + T_2 = 2$ fixed). The following parameter values are used: system size 1200×300, particle number $N_1 = N_2 = 800$ ($\rho_1 = \rho_2 = 0.0022$), mass ratio $M/m = 20$, apex angle $\theta_0 = \pi/18$ and vertical cross-section $L = 1$. All data points are averages over 2000 runs. The lines correspond to the theoretical results (22) and (23).

insight into how the rectified fluctuations result in systematic speed when a temperature gradient is applied.

In figure 10 we have represented the tracks of various motors under other circumstances. In particular, one finds for Triangula and Triangulita that the speed does not depend strongly on the densities. Note however the difference in scaling on both axes: the reason is that the systematic motion, while of the same order of magnitude, is not sustained very long in the denser system.

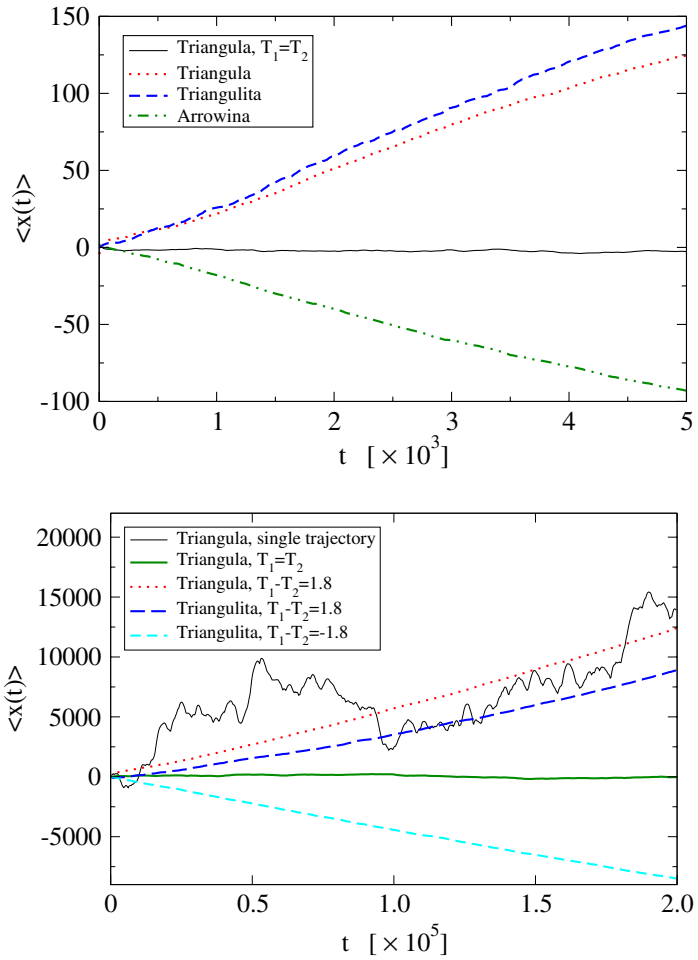

Figure 10. Top, average position (average of 1000 runs) of the different models as a function of time in a system with relative high density ($\rho_1 = \rho_2 \approx 0.3$). The solid line is the equilibrium case ($T_1 = T_2 = 1$) for Triangula. All other curves correspond to non-equilibrium situations, i.e. initial temperatures $T_1 = 1.9$ and $T_2 = 0.1$. The dotted and dashed lines represent the average position of Triangula and Triangulita ($2\theta_0 = \pi/18$, $L = 1$), respectively. The remaining curve shows $\langle x(t)\rangle$ for Arrowina ($\theta = \pi/36$), which has a negative velocity due to its geometric construction. Common parameter values: system size 68 by 20, particle numbers $N_1 = N_2 = 400$ and mass ratio $M/m = 20$. Bottom, position of the motor as a function of time for low densities ($\rho_1 = \rho_2 = 0.0022$). The thin solid curve shows a typical trajectory. All other curves represent the average (of 1000 runs) $\langle x(t)\rangle$. The thick solid line is the equilibrium case ($T_1 = T_2 = 1$) for Triangula. The dotted and dashed curves correspond to the non-equilibrium situation ($T_1 = 1.9$, $T_2 = 0.1$) for Triangula and Triangulita respectively. The situation with switched temperatures for Triangulita is the dashed curve with a negative velocity. Parameter values: system size 1200 by 300, particle numbers $N_1 = N_2 = 800$, mass ratio $M/m = 5$, apex angle $2\theta_0 = \pi/18$ and vertical cross-section $L = 1$.

The reason is that the motor units have in this case a high thermal conductivity so that the system relaxes back to full equilibrium on a much shorter time scale; see also the discussion in section 11.

10. Results for a general convex shape

The above calculation can be repeated for a motor consisting of N rigidly linked closed and convex units, each residing in a separate reservoir filled with gas particles at density ρ_i and temperature T_i, see [27] for the details. One again finds that to lowest order in the perturbation in ε, the Boltzmann equation reduces to a linear Langevin description, $M\partial_t\langle V\rangle = -\gamma\langle V\rangle$ with $\gamma = \sum_i \gamma_i$. Here, γ_i is the linear friction coefficient of the motor unit sitting in gas mixture i:

$$\gamma_i = 4\rho_i L_i \sqrt{\frac{k_B T_i m}{2\pi}} \int_0^{2\pi} \mathrm{d}\theta F_i(\theta) \sin^2\theta. \tag{25}$$

At this order of perturbation, the velocity distribution of the motor is Maxwellian, at the effective temperature:

$$T_{\mathrm{eff}} = \sum_i \gamma_i T_i \Big/ \sum_i \gamma_i. \tag{26}$$

At the next order in the series expansion, one observes that the motor develops a steady-state velocity, namely:

$$\langle V\rangle = \sqrt{\frac{\pi k_B T_{\mathrm{eff}}}{8M}} \sqrt{\frac{m}{M}} \frac{\sum_i S_i\rho_i[(T_i - T_{\mathrm{eff}})/T_{\mathrm{eff}}] \int_0^{2\pi} \mathrm{d}\theta F_i(\theta)\sin^3\theta}{\sum_i S_i\rho_i\sqrt{T_i/T_{\mathrm{eff}}} \int_0^{2\pi} \mathrm{d}\theta F_i(\theta)\sin^2\theta}. \tag{27}$$

This speed is of the order of the thermal speed of the motor, times the expansion parameter $\sqrt{m/M}$, and further multiplied by a factor that depends on the details of the construction. Note that the speed is scale-independent, i.e., independent of the actual size of the motor units: $\langle V\rangle$ is invariant under the rescaling S_i to CS_i (without changing the mass of the motor).

To isolate more clearly the effect of the asymmetry of the motor on its speed, we focus on the case where the units have the same shape in all compartments, i.e. $F_i(\theta) \equiv F(\theta)$ and $S_i \equiv S$. One finds:

$$T_{\mathrm{eff}} = \frac{\sum_i \rho_i T_i^{3/2}}{\sum_i \rho_i \sqrt{T_i}}, \tag{28}$$

and

$$\langle V\rangle = \sqrt{\frac{m}{M}} \sqrt{\frac{\pi k_B T_{\mathrm{eff}}}{8M}} \frac{\sum_i \rho_i((T_i/T_{\mathrm{eff}}) - 1)}{\sum_i \rho_i\sqrt{T_i/T_{\mathrm{eff}}}} \frac{\langle\sin^3\theta\rangle}{\langle\sin^2\theta\rangle}. \tag{29}$$

In this case, T_{eff} is independent of $F(\theta)$ and the drift velocity is proportional to $\langle\sin^3\theta\rangle/\langle\sin^2\theta\rangle$, with the average defined with respect to $F(\theta)$. Since $|\sin^3\theta| \leqslant \sin^2\theta$, the latter ratio is in absolute value always smaller than 1. This limiting value is reached for objects with no special

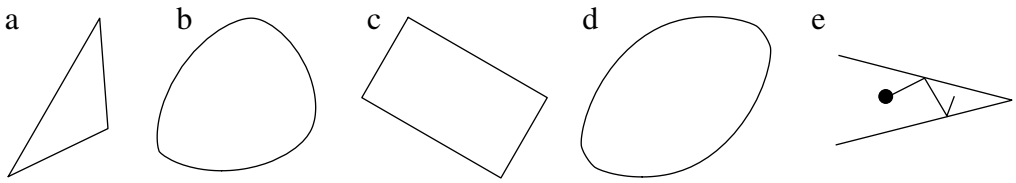

Figure 11. (a), (b) Examples of closed and convex objects for which $\langle \sin^3\theta \rangle = 0$, and consequently—when placed in two reservoirs with different temperature—they generate a very small systematic speed of the order of $(m/M)^{5/2}$. (c), (d) Objects which are invariant under a rotation by 180°. Because of this symmetry, any systematic motion is excluded. (e) Motor unit consisting of an open triangle; systematic motion can appear due to correlated collisions.

shape requirements, except the condition of 'extreme' asymmetry. For example, this limit is, as discussed before, attained for Triangula when $\theta_0 \to 0$. The resulting speed is then very large, i.e., comparable to the thermal speed.

Turning to the complementary question, we wonder what kind of shapes give rise to a small speed. In particular, we establish the condition for the speed given in equation (29) to be equal to zero. We expand the form factor $F(\theta)$, with $\theta \in [0, 2\pi]$ in terms of a Fourier series:

$$F(\theta) = \frac{a_0}{2} + \sum_{n=1}^{\infty} a_n \cos(n\theta) + b_n \sin(n\theta), \tag{30}$$

with

$$a_n = \frac{1}{\pi} \int_0^{2\pi} F(\theta) \cos(n\theta)\, \mathrm{d}\theta, \tag{31}$$

$$b_n = \frac{1}{\pi} \int_0^{2\pi} F(\theta) \sin(n\theta)\, \mathrm{d}\theta. \tag{32}$$

The requirement that the object must be closed implies that $\langle \cos\theta \rangle = \langle \sin\theta \rangle = 0$, or equivalently, $a_1 = b_1 = 0$. Hence the condition of lowest order speed given in equation (29) to be equal to zero, namely $\langle \sin^3\theta \rangle = 0$, is equivalent to $b_3 = 0$ for any closed convex object. Note that such objects need not be symmetric. Two examples are depicted in figures 11(a) and (b). Note also that the above condition $b_3 = 0$ is in general no longer satisfied when one rotates the units of the motor.

We next turn to objects for which the systematic speed is exactly zero, at all orders of perturbation, on the basis of symmetry arguments. Obviously, a motor consisting of symmetric units, i.e., invariant under a reflection about the y-axis, orthogonal on the x-direction, cannot develop a systematic speed. For these objects, F is an even function, $F(\theta) = F(2\pi - \theta) = F(-\theta)$ and consequently $b_n = 0$, $\forall n$. Note again that this property is not necessarily preserved upon rotation of the units.

Going one step further, we identify shapes for which no net motion can be generated even upon rotation of the units. The key is to consider motor units which are invariant under a rotation by 180°. This property is independent of the choice of the x-axis. As we argue below, the average

speed of a motor with such a symmetry has to be exactly zero, whatever the choice of the x-direction. Indeed, a rotation of the motor by 180° implies a reversal of its motion along the x-axis, while on the other hand, since the rotated version is identical to the original motor, the statistics of its motion, and in particular its average speed, are not modified. Hence the average speed has to be zero. Note that units with this symmetry property are described by $F(\theta) = F(\pi - \theta)$ and thus $a_{2n+1} = b_{2n+1} = 0, \forall n$; see figures 11(c) and (d) for some examples.

Finally, it is instructive to apply the above formula to a specific case in which the theory is not valid. Suppose that the units of the motor consist of elements of zero width, e.g., without any interior; see figure 11(e) for an example. Since for any line segment with orientation θ there is an identical segment with orientation $\theta + \pi$, one has $F(\theta) = F(\theta + \pi)$. We conclude that the theoretical speed is exactly zero. However, the Boltzmann equation is no longer correct since a particle can hit the motor unit twice. Indeed, in order to break the left–right symmetry, such line elements have to be curved. As a consequence, the corresponding unit is necessarily a non-convex object. In fact, one expects that such correlated sequences of collisions are responsible for the drift velocities that are observed in this case. This situation is reminiscent of Arrowina, built with completely flat line segments, but with correlated collisions arising from the presence of the reflecting boundary.

11. Thermal conductivity

The above introduced motors cannot run forever, except in the case of infinitely large reservoirs such as those assumed in our theoretical analysis. The reason is clear from both the simulations and the theoretical analysis: the motor, consisting of units residing in reservoirs at different temperatures, will conduct heat, so that in the long run, the system will relax to full thermodynamic equilibrium with equal temperature all over. We will discuss this aspect in more detail for three reasons. Firstly, it was overlooked by Feynman in his otherwise quantitative analysis. Secondly, the irreversible process associated to the heat conductivity is expected to seriously compromise the efficiency of the motor as a thermal engine. Finally, the analytic theory allows a detailed discussion. It vindicates the mesoscopic description given in [9, 10]. Indeed, to lowest order in the expansion in $\sqrt{m/M}$, the theory shows that the speed V of a motor, residing in two reservoirs, obeys a simple linear Langevin equation:

$$M\partial_t V = -(\gamma_1 + \gamma_2)V + \sqrt{2\gamma_1 k_B T_1}\xi_1(t) + \sqrt{2\gamma_2 k_B T_2}\xi_2(t), \qquad \langle \xi_i(t)\xi_j(t')\rangle = \delta(t - t')\delta_{i,j}, \tag{33}$$

where γ_1 and γ_2 are the friction coefficients in compartments 1 and 2, respectively. $\xi_1(t)$ and $\xi_2(t)$ are the Gaussian white fluctuating forces associated to each of the friction processes. In other words, the combined effect of both compartments to the motion can be obtained by adding the separate contributions, which are moreover taken to be linear and of the equilibrium form. The rate of heat transfer $Q_{1\to 2}$ (the heat flux) from compartment 1 to compartment 2 can now be calculated as follows. From (33) one finds that the heat fluxes between the different constituents of the system are given by the following expressions at the steady state:

$$Q_{1\to\text{piston}} = \frac{\gamma_1}{M}[k_B T_1 - M\langle V^2\rangle] = Q_{\text{piston}\to 2} = -\frac{\gamma_2}{M}[k_B T_2 - M\langle V^2\rangle] = Q_{1\to 2}, \tag{34}$$

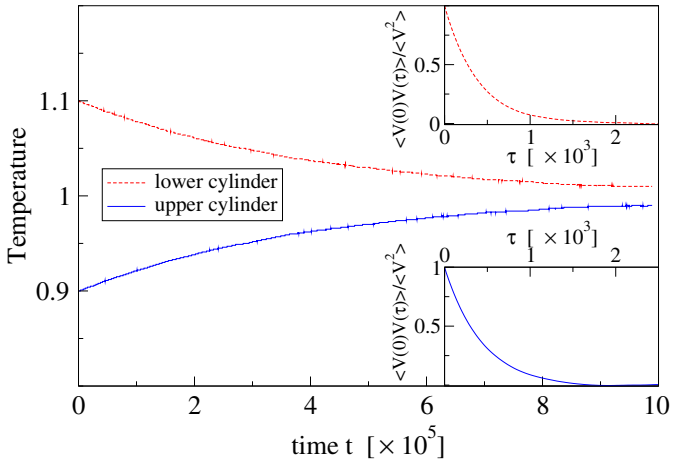

Figure 12. Temperature relaxation in both reservoirs as a result of the thermal contact generated by Triangula. Parameter values: system size 400 × 100, initial temperatures $T_1 = 1.1$ and $T_2 = 0.9$, number of particles $N_1 = N_2 = 900$, mass ratio $M/m = 50$, vertical cross-section $L = 3.1$ and apex angle $2\theta_0 = \pi/18$. Insets: exponential decay of the velocity correlation functions at equilibrium in the upper and lower compartments separately.

implying that the piston thermalizes at the effective temperature $(\gamma_1 T_1 + \gamma_2 T_2)/(\gamma_1 + \gamma_2)$ and that the heat flux obeys a Fourier law:

$$Q_{1\to 2} = \kappa(T_1 - T_2), \qquad \kappa = \frac{k_B \gamma_1 \gamma_2}{M(\gamma_1 + \gamma_2)} \tag{35}$$

with conductivity κ.

To check the validity of this prediction, we turn back to our hard disc simulations. Note that the friction in a single reservoir can be measured by putting the number of particles in the other reservoir equal to zero. In the insets to figure 12, we have included the velocity autocorrelation function of the piston $\langle V(t)V(0)\rangle$ in separate compartments. We observe, to a reasonable approximation, that the velocity correlations decay exponentially with a relaxation time proportional to the piston mass M. From the decay times, we find the friction coefficients $\gamma_1 \approx 0.130$ and $\gamma_2 \approx 0.118$ for the first and second compartments, respectively. According to formula (35), this predicts a conductivity of $\kappa = 1.24 \times 10^{-3}$.

Alternatively, the heat conduction is described by ($N_1 = N_2 = N, k_B = 1$, the kinetic energy of the motor being neglected)

$$Q_{1\to 2} = -\frac{\mathrm{d}}{\mathrm{d}t}U_1 = \frac{\mathrm{d}}{\mathrm{d}t}U_2 = -\frac{1}{2}\frac{\mathrm{d}}{\mathrm{d}t}(U_1 - U_2) = -\frac{N}{2}\frac{\mathrm{d}}{\mathrm{d}t}(T_1 - T_2)\,, \tag{36}$$

together with $Q_{1\to 2} = \kappa\,(T_1 - T_2)$ implying an exponential decay of $T_1 - T_2$ with time constant $N/(2\kappa)$. From the temperature decay of figure 12, a conductivity $\kappa = 1.13 \times 10^{-3}$ is measured, in reasonable agreement with the earlier result based on formula (35).

12. Discussion

We close with a somewhat provocative discussion concerning the nature of the Brownian motor introduced in this paper. We mentioned an essential difference between the Brownian motor considered here and most of the other motors considered in the literature, including the Feynman ratchet, namely that the rectification in our model is not at the expense of momentum exchange with a fixed substrate. Consequently, the motion of the motor must be compensated by a counter motion of the surrounding gas. We now argue that this has a profound implication on the nature of our Brownian motor.

Indeed, the remarkable insight by Onsager, that a small macroscopic disturbance decays in the same way as an equilibrium fluctuation, culminated in the fluctuation dissipation theorem and in the theory of linear irreversible thermodynamics. It shows that macroscopic laws and the fluctuations of the corresponding variables pertaining to the linear regime around equilibrium can be handled in the context of the same macroscopic theory. Most of the Brownian motor models can and have indeed been discussed in such a way, basically involving the calculation of fluxes in response to time-dependent gradients in chemical potential. However, as is clear from the technical discussion of our model, the rectified motion appears beyond linear Langevin theory, at a level where fluctuations and non-linearity are intrinsically intertwined. For this reason we argue that our motor genuinely belongs to the microscopic world, whereas most other models proposed earlier do not.

Acknowledgment

This work was supported in part by the US National Science Foundation under grant nos PHY-0354937 and DMS-0079478.

References

[1] Leff H S and Rex A F 2003 *Maxwell's Demon* (Bristol: Adam Hilger)
[2] Maxwell J C 1871 *Theory of Heat* (London: Longmans Green, republished by Dover in 2001)
[3] von Smoluchowski M 1912 *Physik. Zeitschr.* **13** 1069
[4] Onsager L 1931 *Phys. Rev.* **37** 405
Onsager L 1931 *Phys. Rev.* **38** 2265
[5] Szilard L 1929 *Physik. Zeitschr.* **53** 840
[6] Brillouin L 1951 *J. Appl. Phys.* **22** 334
[7] Landauer R 1961 *IBM J. Res. Dev.* **5** 183
[8] Feynman R P, Leighton R B and Sands M 1963 *The Feynman Lectures on Physics I* (Reading, MA: Addison-Wesley), ch 46
[9] Parrondo J M R and Espagnol P 1996 *Am. J. Phys.* **64** 1125
[10] Sekimoto K 1997 *J. Phys. Soc. Japan* **66** 1234
[11] Oster G 2002 *Nature* **417** 25
Taton T A 2001 *Nature* **412** 491
Kelly T R, Sestelo J P and Tellitu I 1998 *J. Org. Chem.* **63** 3655
[12] Gaspard P 1998 *Chaos, Scattering, and Statistical Mechanics* (Cambridge: Cambridge University Press)
[13] Evans D J and Searles D J 2002 *Adv. Phys.* **51** 1529
[14] Rapaport D C 1995 *The Art of Molecular Dynamics Simulation* (Cambridge: Cambridge University Press)

[15] Reimann P 2002 *Phys. Rep.* **361** 57
Astumian R D and Hanggi P 2002 *Phys. Today* **55** 33
Linke H (ed) 2002 *Ratchets: Basics, Experiments and Applications*, *Appl. Phys.* A **75**
[16] Pesz K, Gabrys B J and Bartkiewicz S J 2002 *Phys. Rev.* E **66** 61103
Denur J 2002 *AIP Conf. Proc.* **643** 326
Velasco S, Roco J M M, Medina A and Hernandez A C 2001 *J. Phys. D: Appl. Phys.* **34** 1000
Abbott D, Davis B R and Parrondo J M R 2000 *AIP Conf. Proc.* **511** 213
Luczka J 1999 *Physica* A **274** 200
Sakaguchi H 1998 *J. Phys. Soc. Japan* **67** 709
Magnasco M O and Stolovitzky G 1998 *J. Stat. Phys.* **93** 615
Jarzynski C and Mazonka O 1999 *Phys. Rev.* E **59** 6448
[17] Skordos P A and Zurek W H 1992 *Am. J. Phys.* **60** 876
Skordos P A 1993 *Phys. Rev.* E **48** 777
[18] Zhang K and Zhang K 1992 *Phys. Rev.* A **46** 4598
[19] Gruber Ch and Piasecki J 1999 *Physica* A **268** 412
[20] Kestemont E, Van den Broeck C and Mansour M M 2000 *Europhys. Lett.* **49** 143
[21] Handrich K and Ludwig F P 1997 *J. Stat. Phys.* **86** 1067
[22] Van den Broeck C, Kawai R and Meurs P 2004 *Phys. Rev. Lett.* **93** 090601
[23] Michaels I A and Oppenheim I 1975 *Physica* A **81** 221
[24] Dorfman J R, Van Beijeren H and McClure C F 1976 *Arch. Mech.* **28** 333
[25] Van Kampen N G 1981 *Stochastic Processes in Physics and Chemistry* (Amsterdam: North-Holland)
[26] Bird G M 1976 *Molecular Gas Dynamics* (Oxford: Clarendon)
[27] Meurs P, Van den Broeck C and Garcia A 2004 *Phys. Rev.* E **70** 1